ChemComm

Accepted Manuscript

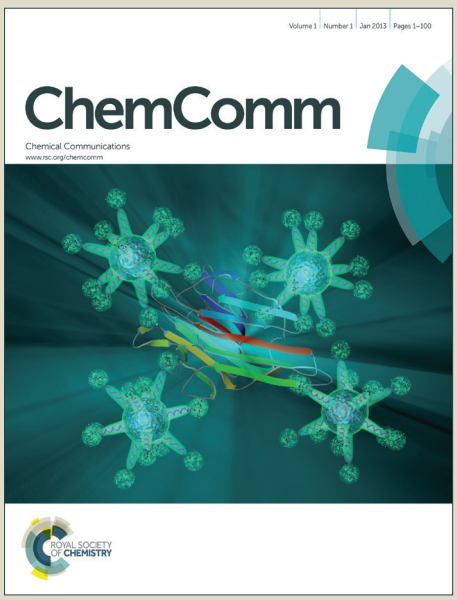

ROYAL SOCIETY OF CHEMISTRY

www.rsc.org/chemcomm

Chemical Communications

COMMUNICATION

A Highly N-Doped Carbon Phase "Dressing" of Macroscopic Supports for Catalytic Applications†

Received 00th January 20xx,
Accepted 00th January 20xx

DOI: 10.1039/x0xx00000x

www.rsc.org/

Housseinou Ba,[a,c,§] Yuefeng Liu,[a,§] Lai Truong-Phuoc,[a] Cuong Duong-Viet,[a] Xiaoke Mu,[a] Won Hui Doh,[a] Tung Tran-Thanh,[a] Walid Baaziz,[a] Lam Nguyen-Dinh,[b] Jean-Mario Nhut,[a] Izabela Janowska,[a] Dominique Begin,[a] Spiridon Zafeiratos,[a] Pascal Granger,[c] Giulia Tuci,[d] Giuliano Giambastiani,[d,f,*] Florian Banhart,[e] Marc J. Ledoux[a] and Cuong Pham-Huu[a,*]

The straightforward "dressing" of macroscopically shaped supports (*i.e.* β-SiC and α-Al_2O_3) with a mesoporous and highly nitrogen-doped carbon-phase starting from food-processing raw materials is described. The as-prepared composites serve as highly efficient and selective metal-free catalysts for promoting industrial key-processes at the heart of renewable energy technology and environmental protection.

One main challenge of modern and sustainable catalysis is to re-think fundamental metal-based catalytic processes while eliminating critical raw components like expensive noble metals. The exploitation of tailored metal-free catalytic architectures designed and fabricated from cheap and easily accessible building blocks may represent a valuable and green alternative. Nitrogen-doped 1D and 2D carbon nanomaterials (N-CNMs), have emerged in the last decade as effective metal-free systems, capable of promoting a high number of catalytic processes.[1-8] Since the pioneering work by Gong *et al.*,[1] independent studies have demonstrated how the inclusion of nitrogen(s) in the honeycomb carbon structure breaks the electroneutrality of the C_{sp2} network[9,10] and generates charged active sites.[11] Their presence plays a pivotal role on the ultimate material catalytic activity, sometimes offering performance comparable or even better than that observed with classical metal-based systems. Among the synthetic approaches known for the production of N-CNMs systems, Chemical Vapour Deposition (CVD) still remains the most popular and widely used technique. At odds with its feasibility, CVD suffers from a number of serious drawbacks: (i) the use of nitrogen precursors with relatively high toxicity [*i.e.* pyridine,[12,13] acetonitrile,[14] ammonia[15,16]]; (ii) tricky reaction environments based on hydrocarbons and/or hydrogen atmosphere (which typically necessitate of specific safety operative precautions); (iii) high operation temperatures. In addition, significant losses of the N- and C-containing gaseous reagents throughout the synthesis (including their partial thermal decomposition into waste and toxic by-products) denote an invariably low atom efficiency of the CVD technique. All these aspect taken together make CVD rather unattractive, because of its heavy environmental impact and unsustainable production costs.

In recent years, the joint efforts of chemists, physicists and engineers have paved the way to the development of a number of innovative synthetic tools for the efficient and controlled carbon nanomaterials N-decoration/doping.[11,17,18] Despite of the potential interest for N-doped CNMs as metal-free catalysts in a series of industrially relevant processes, none of the emerging synthetic technologies has really fulfilled the requirements for their sustainable and environmentally friendly large-scale production. In addition, the difficult CNMs handling, caused by their prevalent powdery texture has dramatically limited their extensive exploitation as catalysts in both gas- and liquid phase processes.

This contribution describes a straightforward and environmentally benign methodology for the preparation of highly N-doped CNMs starting from non-toxic, raw and abundant organic building blocks. A shape-adaptable, highly N-doped mesoporous carbon phase is properly grown as a truly metal-free "catalytic clothing" at the surface of macroscopically shaped supports. Various matrices based on silicon carbide (β-SiC)[19,20] in the form of powder (< 40 µm), grains (150 - 400 µm), extrudates (1 x 2 mm) and foams (from mm to cm) or α-Al_2O_3 beads (mm), are selected as catalyst scaffolds (Fig. S2†).

Ammonium carbonate [$(NH_4)_2CO_3$], citric acid ($C_6H_8O_7$) and L-glucose are the non-toxic foodstuff constituents of a homogeneous aqueous pre-catalytic phase to be used as an impregnating solution for the catalysts scaffolds to be soaked.[21,22] Successive thermal treatments of the impregnated β-SiC (or α-Al_2O_3) supports generate highly N-doped, carbonaceous surface coatings featured by Specific Surface

a. Institut de Chimie et Procédés pour l'Energie, l'Environnement et la Santé (ICPEES), ECPM, UMR 7515 CNRS-Université de Strasbourg, 25, rue Becquerel, 67087 Strasbourg Cedex 02, France. E.mail: cuong.pham-huu@unistra.fr
b. The University of Da-Nang, University of Science and Technology, 54 Nguyen Luong Bang, Da-Nang, Viet-Nam.
c. Unité de Catalyse et Chimie du Solide (UCCS), UMR 8181 du CNRS-Université de Lille-1, Bâtiment C3, Université Lille-1, 59655 Villeneuve d'Ascq Cedex, France.
d. Institute of Chemistry of OrganoMetallic Compounds, ICCOM-CNR and Consorzio INSTM, Via Madonna del Piano, 10 – 50019, Sesto F.no, Florence, Italy. E-mail: giuliano.giambastiani@iccom.cnr.it
e. Institut de Physique et Chimie des Matériaux de Strasbourg (IPCMS), UMR 7504 CNRS- University of Strasbourg, 23, rue du Loess, 67034 Strasbourg Cedex 02, France.
f. Kazan Federal University, 420008 Kazan, Russian Federation.
§ These authors contributed equally to the work

† Electronic Supplementary Information (ESI) available: Experimental procedure, materials and methods, Table S1, ^1H and $^{13}C\{^1H\}$ NMR spectra, SEM images, HR TEM and experimental catalytic details on Fig. S1-S13. See DOI: 10.1039/x0xx00000x

Areas (SSA) and basicity higher than those of the pristine host matrices (*vide infra*).

A first thermal treatment at 130 °C in air (drying) produces a thin pre-catalytic coating of the host scaffolds essentially made of D-glucose and basic ammonium citrate (Figs. 1 and S1†). The soaking/drying treatment can be repeated for a number of times at will, thus increasing the thickness of the pre-catalytic deposit. The coating C/N ratio can also be tuned by adopting various compositions of the impregnating phase [*i.e.* solutions at various D-glucose/$(NH_4)_2CO_3$/citric acid molar ratios] during the successive soaking/drying cycles (Table S1†, entries 1 *vs.* 4 and 2 *vs.* 5).

Two final treatments, at 450 °C under air and at 900 °C under inert atmosphere (annealing), "dress" the support with a N-doped mesoporous carbon phase (N@C) (Figs. 1, S2†).[22]

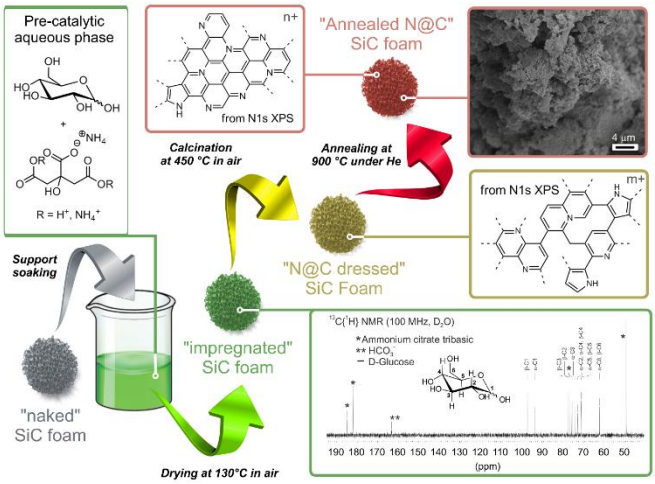

Fig. 1 Synthesis of a highly N-doped carbon-based coating (N@C) on a model macroscopically shaped host matrix (SiC foam). Arrows refer to the four sequential synthetic steps; from the material soaking and drying up to its calcination at 450 °C in air followed by annealing at 900 °C under inert atmosphere. The N@C surface coating composition is determined by either $^{13}C\{^1H\}$ NMR spectroscopy (for the water-soluble pre-catalytic phase at the surface of the impregnated composite) and N1s XPS analysis for the samples treated at 450 and 900 °C, respectively (see also Fig. 2). NMR spectrum refers to a model pre-catalytic phase prepared dissolving 2g of D-Glucose, 3g of citric acid and 2.3g of $(NH_4)_2CO_3$ in 500 mL of ultrapure Milli-Q water and repeating the soaking/drying phase twice. SEM image refers to the typical porous texture of the N@C phase after material annealing.

Thermal treatments induce polymerization/condensation processes that enhance the N@C phase adhesion to the host scaffold while improving its ultimate electrical and thermal conductivity. D-Glucose represents the main source of carbon in the process, while the basic ammonium citrate (in the forms of tri-, di- or mono-basic, depending on the ammonium carbonate/citric acid molar ratio used) plays the double role of N-reservoir and pore forming agent ("leavening" agent; Fig. S3†) throughout the two last thermal phases.

The as-prepared composites are conventionally designated as follows: $^{A}N@C/(supp)_x^y$, where the superscript "A" denotes "annealed samples" (900°C under inert atmosphere), "N@C/(supp)" stands for a composite made of a catalyst support (supp = β-SiC or α-Al_2O_3) coated with the N@C active-phase, the "X" subscript illustrates the pristine support texture (P = powder; G = grains; E = extrudates; F = foams) and the "Y" superscript displays the number of performed impregnation/drying cycles.

The N@C composites show higher SSA values compared to the respective pristine supports (Figs. S4†, S5†and Table S1†). For the model $^{A}N@C/(SiC)_E^2$ composite [**V**] (Table S1†, entry 5), the SSA increases up to five times above its original value (Figs. S4† and S5†, SSA (SiC_E): 30 m^2/g *vs.* SSA [$^{A}N@C/(SiC)_E^2$]: 144 m^2/g).[22] A higher basicity of the N@C composites, compared to the bare catalyst supports, has also been measured. The pH value of an aqueous dispersion of [**III**] (Table S1†, entry 3) grows to pH 9.6 from pH 6.7 of the bare SiC_P support (Fig. S6†).[23]

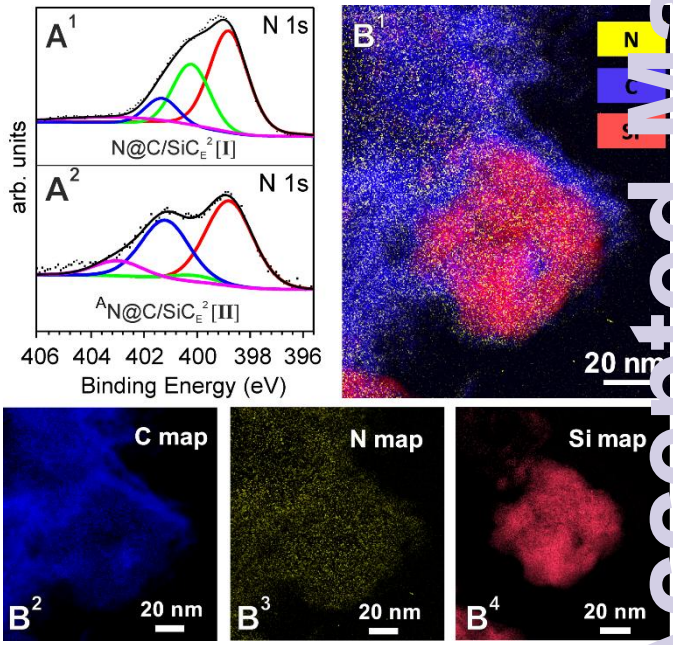

Fig. 2 (**A**) High-resolution N 1s XPS spectra of two samples prepared from extrudate SiC supports (Table S1†, entries 1-2). SiC_E undergoes two impregnation/drying cycles before being heated at 450 °C in air for 2h (**A¹**) and annealed at 900 °C under He atmosphere for 1h (**A²**). (**B**) STEM-EELS analysis of the annealed sample [**III**] (Table S1†, entry 3). Colours labelling in the elemental map **B¹** are: yellow for Nitrogen, red for Silicon and blue for Carbon. Separate element maps are shown in Fig. **B²** (carbon), **B³** (nitrogen) and **B⁴** (silicon).

Such a distinctive feature, not observed in traditionally prepared (CVD) N-doped CNMs, is ascribed to an exceptionally high density of surface-exposed basic N-sites. N 1s XPS analysis provides details on the nature of the N-species available at the N@C phase and how they change throughout the successive thermal treatments. As Fig. 2 [**A¹** *vs.* **A²**] shows, the model composites [**I**] and [**II**] (Table S1†) present three and two main components, respectively, along with a common minor shoulder at higher binding energies (403,1 eV ascribed to N-oxidized species). Curve fitting for sample [**I**] is consistent with the presence of pyridinic (398.8 eV – red line; 55 %), pyrrolic (400.2 eV – green curve; 29 %) and quaternary (401.3 eV; 16 %) nitrogens, respectively [Fig. 2, **A¹**]. Thermal annealing translates

into an N@C phase made of N-pyridinic (398.8 eV; 43 %) and quaternary N-groups (401.3 eV; 37 %) almost exclusively (Fig. 2, **A²** Table S1†, entries 1 *vs.* 2 and 4 *vs.* 5). Thermogravimetric (TGA, Fig. S7†) and elemental analyses (Table S1†) are then used to determine the N wt. % at the N@C phase for each sample[24] (Table S1†). Measurements have unveiled remarkably high N-contents (normalized to the N@C mass deposit on the catalyst support): 32 wt. % (Table S1†, entry 1) for samples treated in air at 450°C and 23 wt. % for annealed composites (Table S1†, entry 3). Electron energy-loss spectroscopy (EELS) in High-Resolution STEM (STEM-EELS) analysis conducted on the model composite [**III**] (Table S1†, entry 3) confirms the high N-concentration at the material topmost surface [Figs. 2, **B¹**-**B⁴** and S8†, S9†][22].

These unique material properties make the N@C-based macroscopic composites ideal single-phase catalysts to perform a number of industrially relevant liquid-phase and gas-phase catalytic transformations acting as heterogeneous metal-free systems.

As a first catalytic trial, a Nafion®-based ink of **III** (Table S1†, entry 3) is employed in the model liquid-phase electrochemical oxygen reduction reaction (ORR) under alkaline environment (KOH 0.1 M). Fig. 3 shows its remarkable catalytic performance [rotating ring-disk electrode (RRDE) measurements] along with that of a model 20 wt. % Pt/C catalyst (Nafion®-based ink of 20 wt. % of Pt on Vulcan® XC72) and those of the respective bare supports under identical conditions (Nafion®-based ink of SiCp and Vulcan® XC72).

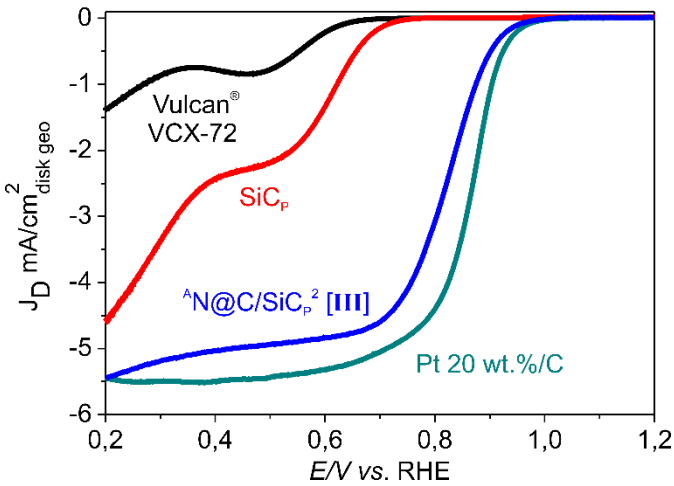

Fig. 3 RRDE potential curves at 25 °C for ORR in O_2 saturated 0.1 M KOH solution, recorded by a rotating ring-disk GC electrode operating at 1600 rpm [GC disk, A = 0.238 cm²]. Curves refer to [**III**] (< 40 µm, 450 µg.cm^{-2}, blue line), Vulcan® XC72 (100 µg cm^{-2}, black line), 20 wt. % Pt/C (Vulcan® XC72, 25 µgPt cm^{-2}, light blue line) and SiC_P (< 40 µm, 450 µg cm^{-2}, red line).

The Koutecky-Levich (K-L) plots of both metal-free and Pt/C-based electrocatalysts, as obtained from the respective linear sweep voltammograms (LSVs) at 0.4 V, present similar curve slopes consistent with a four-electron mechanism operating on both systems (Fig. S10A†). Further proof of evidence of a prevalent four-electron mechanism is given by the low Pt-ring currents measured on both systems at the RRDE (due to the % production of H_2O_2, Fig. S10B†). According to these data, the average number of electrons transferred (n) per mol of O_2 are calculated in 3.6 and 4 on **III** and on the Pt/C catalysts, respectively. The onset potential values (E_{on}) are very close to each other (~ 1V), while the half-wave potential ($E_{1/2}$) measured on **III** is fixed about 45 mV down (overpotential) to that of the Pt/C based system. Overall, $E_{1/2}$ and current density values (J) measured at 0.9 V reveal only a slightly reduced catalytic performance of the metal-free system compared with the classical Pt-containing one. On the other hand, a remarkably higher stability of **III** compared to that of the Pt/C-based system is observed for long-term cycling RRDE tests (measurements in the 0.6 - 1.0 V range at 100 mVs^{-1}, 1600 rpm in 0.1 M KOH at 25°C). As Fig. S11† shows, catalyst **III** retains about 80% of its initial ORR activity after 1500 cycles, whereas that of the Pt/C-based system drops down to 65% of its initial catalytic performance under the same experimental conditions.

The oxidation of H_2S residues from refinery tail-gas effluents is selected as a model high-temperature gas-phase reaction to be accomplished with the developed metal-free catalysts technology, in agreement with the current environmental legislation. The extruded SiC-based composite **II** (Table S1†, entry 2) is selected as catalytic candidate for this process. As Fig. 4 shows, at T = 210 °C with a O_2/H_2S molar ratio of 2.5 and a 0.3 h^{-1} Weight Hourly Space effluent Velocity (WHSV), **II** exhibits a remarkably high desulfurization activity (> 97% of H_2S conversion) with a sulfur selectivity close to 70 %. Notably, no catalyst deactivation takes place under these severe conditions even after prolonged (> 100 h) reaction times that mirror with only negligible leaching and decomposition effects of the N@C active phase. For the sake of completeness, the model Fe_2O_3/SiC catalyst is selected as a reference desulfurization benchmark,[25,26] and tested under comparative experimental conditions. Despite its high selectivity (> 90%), the Fe_2O_3-based system shows a markedly lower desulfurization activity when compared with **II** (Fig. S12†). The high surface density of active sites at the N@C-based catalyst is likely responsible for the higher H_2S conversion measured respect to the Fe-based system (Fig. S12†).

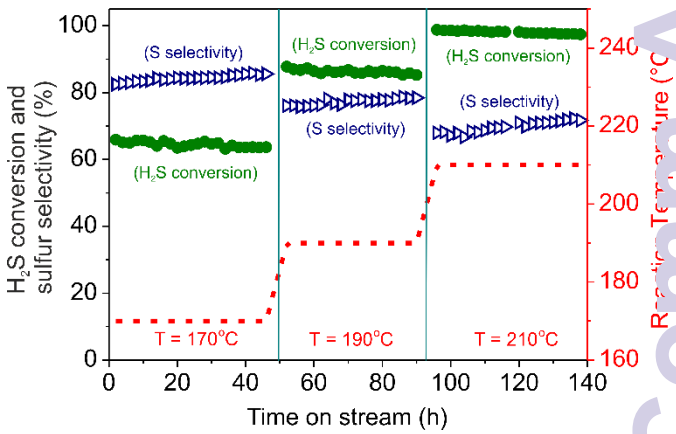

Fig. 4 Desulfurization performance on **II** as a function of the reaction conditions (1g of **II**, O_2/H_2S molar ratio = 2.5, WHSV = 0.3 h^{-1}).

The absence of metal nanoparticles in the catalyst active phase (N@C) also prevents undesired sintering side-effects classically responsible for catalysts deactivation in metal-containing systems. On the other hand, the combination of a high active sites density at the material topmost surface with the porous structure of the SiC matrix (ideal for optimal reagents mixing degree and catalyst/reagent

contacts) translates into a moderate selectivity towards elemental sulfur. Improved catalyst performance (compared to the Fe_2O_3-based system), in terms of both H_2S conversion and S selectivity, is given by an N@C active phase grown on α-Al_2O_3 beads as an alternative support with a lower surface area (Table S1†, entry 6).

As shown in Fig. S13†, catalyst **VI** provides a remarkably high desulfurization activity (over 70% of H_2S conversion) with a sulfur selectivity close to 90% under running conditions. In spite of slightly lower H_2S conversion, selectivity higher than 90% can be also achieved with the same catalyst through a reduction of the O_2/H_2S molar ratio (O_2/H_2S : 2.5 *vs*. 1).

Conclusions

In summary, the proposed methodology offers a sustainable and truly metal-free approach to the generation of highly adaptable N-doped, carbon porous active phases (N@C) capable of "dressing" different macroscopic host scaffolds. Depending on the downstream catalytic application of the final composites (gas-phase or liquid-phase reactors), the mesoporous N@C carbon phases are grown in the form of tight coatings on different supports: powders, grains, beads, extrudates and foams. At odds with the classical CVD technique, C and N sources for this methodology are cheap solid feedstock, neither toxic nor dangerous or explosive. Most importantly, their conversion into highly N-doped porous carbon phases meets the requirements of atom efficiency, negligible environmental impact and low production costs necessary for the industrial exploitation of a truly metal-free technology.

The successful use of these metal-free N@C catalysts in two model and fundamental catalytic transformations is finally described: 1) the liquid-phase electrochemical oxygen reduction reaction in alkaline environment and 2) the high temperature gas-phase H_2S partial oxidation to elemental sulfur. For both processes, the N@C composites appear as ideal catalyst candidates capable of offering high (and to some extent better) catalytic performance and long-term stability compared to the classical metal-based systems (including platinum-group-metals - PGMs) of the state-of-the-art. Finally, the easy and cost-efficient up-scale synthesis of stable N@C active phases on different macroscopic host supports paves the way to a further material exploitation in other processes where the combination of exposed basic sites with good electrical conductivity and thermal stability are essential pre-requisites for high catalytic performances.

Acknowledgments

This work was financially supported by the Freecats FP7 European project (contract n° NMP3-SL-2012-280658). The authors would like to thank Sicat Co. (www.sicatcatalyst.com) for supplying the SiC supports within the framework of the above mentioned project.

Notes and references

1 K. Gong, F. Du, Z. Xia, M. Durstock, L. Dai, *Science*, 2009, **323**, 760.
2 Y. Li, W. Zhou, H. Wang, L. Xie, Y. Liang, F. Wei, J.-C. Idrobo, S. J. Pennycook, H. Dai, *Nat. Nanotechnol*., 2012, **7**, 394.
3 R. Liu, D. Wu, X. Feng, K. Müllen, *Angew. Chem. Int. Ed*., 2010, **49**, 2565.
4 K. Chizari, A. Deneuve, O. Ersen, I. Florea, Y. Liu, J. Edouard, I. Janowska, D. Begin, C. Pham-Huu, *ChemSusChem*, 2012, **5**, 102.
5 D. S. Su, S. Perathoner, G. Centi, *Chem. Rev*., 2013, **113**, 5782.
6 F. Bonaccorso, L. Colombo, G. Yu, M. Stoller, V. Tozzini, A. C. Ferrari, R. S. Ruoff, V. Pellegrini, *Science*, 2015, **347**, 1246501.
7 S. Yang, X. Feng, X. Wang, K. Müllen, *Angew. Chem. Int. Ed*., 2011, **50**, 5339.
8 X. Li, X. Pan, L. Yu, P. Ren, X. Wu, L. Sun, F. Jiao, X. Bao, *Nat. Commun*., 2014, **5**, ncomms4688-1.
9 C. Zhou, J. Kong, E. Yenilmez, H. Dai, *Science*, 2000, **290**, 1552.
10 X. Wang, X. Li, L. Zhang, Y. Yoon, P. K. Weber, H. Wang, J. Guo, H. Dai, *Science*, 2009, **324**, 768.
11 G. Tuci, C. Zafferoni, A. Rossin, A. Milella, L. Luconi, M. Innocenti, L. Truong Phuoc, C. Duong-Viet, C. Pham-Huu, G. Giambastiani, *Chem. Mater*., 2014, **26**, 3460.
12 C. Shan, W. Zhao, X. L. Lu, D. J. O'Brien, Y. Li, Z. Cao, A. L. Elias, R. Cruz-Silva, M. Terrones, B. Wei, J. Suhr, *Nano Lett*., 2013, **13**, 5514.
13 Y. Xue, B. Wu, L. Jiang, Y. Guo, L. Huang, J. Chen, J. Tan, D. Geng, B. Luo, W. Hu, G. Yu, Y. Liu, *J. Am. Chem. Soc*., 2012, **134**, 11060.
14 Y. Xia, G. S. Walker, D. M. Grant, R. Mokaya, *J. Am. Chem. Soc*., 2009, **131**, 16493.
15 T. Susi, A. Kaskela, Z. Zhu, P. Ayala, R. Arenal, Y. Tian, P. Laiho, J. Mali, A. G. Nasibulin, H. Jiang, G. Lanzani, O. Stephan, K. Laasonen, T. Pichler, A. Loiseau, E. I. Kauppinen, *Chem. Mater*., 2011, **23**, 2201
16 L. Qu, Y. Liu, J.-B. Baek, L. Dai, *ACS Nano*, 2010, **4**, 1321.
17 W. He, C. Jiang, J. Wang, L. Lu, *Angew. Chem. Int. Ed*., 2014, **53**, 9503.
18 Y. Meng, X. Zou, X. Huang, A. Goswami, Z. Liu, T. Asefa, *Adv. Mater*., 2014, **26**, 6510.
19 Y. Liu, O. Ersen, C. Meny, F. Luck, C. Pham-Huu, *ChemSusChem*, 2014, **7**, 1218.
20 P. Nguyen, C. Pham, *Appl. Catal. A-Gen*., 2011, **391**, 443.
21 C. Pham-Huu, G. Giambastiani, Y. Liu, H. Ba, L. Nguyen-Dinh, J.-M. Nhut, Eur. Pat. Appl. No. EP 15-152038 (2015).
22 Details available on the ESI material.
23 R. Arrigo, M. Hävecker, S. Wrabetz, R. Blume, M. Lerch, J. McGregor, E. P. J. Parrott, J. A. Zeitler, L. F. Gladden, A. Knop-Gericke, R. Schlögl, D. S. Su, *J. Am. Chem. Soc.*, 2010, **132**, 9616.
24 N-content as calculated from the XPS analysis is invariably underestimated as a consequence of unpredictable contributions from Si and C arising from the SiC scaffold background
25 N. Keller, C. Pham-Huu, M. J. Ledoux, *Appl. Catal. A-Gen*, 2001, **217**, 205.
26 P. Nguyen, D. Edouard, J.-M. Nhut, M. J. Ledoux, C. Pham, C. Pham-Huu, *Appl. Catal. B-Gen*., 2007, **76**, 300.